Available online at www.sciencedirect.com

ScienceDirect

Ceramics International 40 (2014) 893–900

CERAMICS INTERNATIONAL

www.elsevier.com/locate/ceramint

Powder injection molding process design for UAV engine components using nanoscale silicon nitride powders

Juergen Lenz[a], Ravi Kumar Enneti[b], Seong-Jin Park[c], Sundar V. Atre[a,*]

[a]Oregon State University, Corvallis, OR, USA
[b]Global Tungsten Products, Towanda, PA, USA
[c]Pohang University of Science & Technology, Pohang, Republic of Korea

Received 11 June 2013; received in revised form 21 June 2013; accepted 21 June 2013
Available online 5 July 2013

Abstract

The feasibility of powder injection molding to fabricate silicon nitride engine components was evaluated in the presented study. Experiments were carried out on a feedstock consisting of nanoscale silicon nitride powders mixed with magnesia, yttria and a paraffin wax–polypropylene binder system. The measured rheological and thermal properties of feedstock were used to simulate the flow of material during injection molding of a combustion engine for an unmanned aerial vehicle (UAV). Simulations based on the Box–Behnken design were used to identify the critical parameters affecting the injection molding process. The simulation results identified melt temperature as the dominant factor affecting the injection pressure, clamp force, shear stress, sink mark depth, temperature at flow front and volumetric shrinkage. Injection time was found to be the dominant factor affecting the bulk temperature and time at the end of the packing. The optimal injection molding parameters were further estimated using a non-linear programming (NLP) model. It is expected that the engineering community can use the simulation techniques discussed in the study to identify optimum processing conditions for fabricating the complex engine parts, thereby avoiding iterative expensive and time-consuming trials.

Keywords: Injection molding; Simulation; Box–Behnken design; Non-linear programming (NLP) model

1. Introduction

Significant research efforts are being focused since past few decades in developing higher performance and efficient engine components for unmanned aerial vehicles (UAV). The engine efficiency is extremely critical for the UAV application as higher efficiency will directly result in extending the distance of the flight. The use of engine components made from ceramics enable higher operating temperature of the engines resulting in higher efficiency. An increase in efficiency of 7–12% has been previously reported by coating various engine components with ceramics [1–3].

Silicon nitride (Si_3N_4) has a combination of useful attributes such as relatively low density, high temperature stability, high creep resistance, low thermal coefficient of expansion, chemical stability, and high strength at elevated temperatures which makes it a strong candidate for manufacturing high performance UAV engine components [4–6]. However, the high hardness of Si_3N_4 makes machining of the complex engine components difficult and expensive thus restricting the available manufacturing technologies to produce the parts economically.

Powder injection molding (PIM) has a proven record for the cost-effective manufacturing of complex net-shape parts [7–9]. Consequently, PIM was selected as a potential technology to fabricate Si_3N_4 engine components in this study. Several prototypes of Si_3N_4 engine components have been previously fabricated using PIM [1,3,10]. However, the engine dimensions are typically larger and therefore more susceptible to defects during processing. Further, the absence of human payload in the present UAV application makes the exploration of Si_3N_4 and PIM a potentially safer and significantly less

*Corresponding author. Tel.: +1 541 737 8272.
E-mail addresses: ravienneti@gmail.com (R.K. Enneti), sundar.atre@oregonstate.edu (S.V. Atre).

0272-8842/$ - see front matter © 2013 Elsevier Ltd and Techna Group S.r.l. All rights reserved.
http://dx.doi.org/10.1016/j.ceramint.2013.06.084

expensive fit. Finally, the lack of reliable feedstock material property data and simulation tools for performing mold and part design has been a major factor in limiting the development and growth of the technology.

The feasibility of PIM to fabricate Si_3N_4 engine components was evaluated in the presented study. A feedstock was developed consisting of nanoscale Si_3N_4 powders mixed with nanoscale magnesia and yttria powders as sintering aids. Nanoscale powders were selected in order to determine their suitability for enhancing their densification and mechanical properties at lower sintering temperatures, in the absence of external pressure. The binder system was based on a mixture of paraffin wax, stearic acid and polypropylene. Several rheological and thermal properties of the feedstock were measured and used to simulate the flow of material during injection molding of a UAV combustion engine. The critical material and process parameters affecting the quality of injection molding process were identified based on the Box–Behnken design method. The Box–Behnken method is a response surface design and is relatively inexpensive method compared to central composite designs [11–21]. The response surface designs fit a quadratic model to predict the response as a curved function of the factors. The developed quadratic model is used to identify operating conditions with less variations and higher robustness. As per authors′ knowledge, simulations based on the Box–Behnken design are reported for the first time in the current study for ceramic injection molding process. Consequently, the design protocol and the results presented here will assist in successful fabrication of combustion engines by the ceramic injection molding process. It is expected that the engineering community can use the simulation techniques discussed in the study to identify optimum processing conditions for fabricating the complex engine parts, thereby avoiding iterative expensive and time-consuming trials.

2. Feedstock characterization

Commercially available Si_3N_4 powders (median particle size: 130 and 20 nm size mixed in a ratio of 95:5 wt%) were blended with magnesia 4 wt% (median particle size: 50 nm) and 5 wt% yttria (median particle size: 70 nm), and multi-component polymer systems based on paraffin wax, polypropylene were used as feedstock components. The sintering aids were selected based on earlier reports on their suitability for obtaining competitive mechanical properties by pressureless sintering [22]. The Si_3N_4 feedstock was prepared by mixing powder and binder components in a co-rotating 27 mm twin-screw extruder (Entek). The extruded feedstock with a powder content of 80 wt% (as confirmed by thermogravimetric

Table 1
Summary of the feedstock properties used as input data for the simulation studies.

Property	Measurement technique	Data
Rheological constants	Capillary rheometry (Rheograph 2003, Goettfert) ASTM D3835	n (Slope of shear-thinning curve): 0.06 τ^* (Weissenberg–Rabinowitsch correction): 130 kPa D_1 (scale factor for viscosity): 1.0E+23 Pa-s A_1 (WLF temperature shift factor): 42.28 D_2 (glass transition temperature): 373 K A_2 (WLF temperature shift factor): 51.6 K
Thermal conductivity data	K-system II thermal conductivity ASTM D5930	184 °C: 1.13 W/m-K 154 °C: 1.53 W/m-K 123 °C: 1.28 W/m-K 93 °C: 1.50 W/m-K 62 °C: 1.43 W/m-K
Specific heat data	DSC7, Perkin Elmer	170 °C: 1163 J/kg-K 111 °C: 1059 J/kg-K 58 °C: 1009 J/kg-K 47 °C: 1698 J/kg-K 24 °C: 1004 J/kg-K 17 °C: 913 J/kg-K 0 °C: 791 J/kg-K
PVT coefficients	Gnomix PVT apparatus in ASTM D792	b_5 (crystallization temperature): 336.15 K, b_6 (pressure sensitivity to b_5): 1.73×10^{-7} K/Pa b_{1m} (Tait constant for melt): 5.0×10^{-4} m^3/kg b_{2m} (Tait constant for melt): 2.04×10^{-7} m^3/kg-K b_{3m} (Tait constant for melt): 2.63×10^{8} 08 Pa b_{4m} (Tait constant for melt): 3.61×10^{-3}/K b_{1s} (Tait constant for solid): 4.0×10^{-4} m^3/kg b_{2s} (Tait constant for solid): 1.04×10^{-7} m^3/kg-K, b_{3s} (Tait constant for solid): 7.70×10^{8} Pa b_{4s} (Tait constant for solid): 5.1×10^{-4}/K b_7 (Tait constant for melt transition): 1.61×10^{-5} m^3/kg b_8 (Tait constant for melt transition): 3.8×10^{-2} 1/K b_9 (Tait constant for melt transition): 1.44×10^{8} 1/Pa

analysis) was pelletized and the rheological properties, thermal conductivity, specific heat, PVT properties were measured. The method and equipment used for measuring the properties are summarized in Table 1. The measured feedstock properties were used an input for simulation studies. A rectangle shaped multiple channels test part was processed to evaluate the quality of the developed feedstock. The test part was successfully injection molded and debound. Subsequently, sintering was performed in nitrogen at 1850 °C without the formation of any major defects. A photograph of the green and sintered test parts is shown in Fig. 1. The SEM images of the green and sintered microstructures are shown in Fig. 2. The green microstructures show the discrete powders embedded in the binder matrix. The grain growth and rod-shaped orientation in the microstructure indicates a complete transformation of the β-phase Si_3N_4. The rod shaped microstructure is formed *in situ* during liquid phase sintering due to anisotropic grain growth and is identified to be highly beneficial in improving the fracture toughness of Si_3N_4 [23–26]. A high fracture toughness of 10 MPa $m^{1/2}$ was achieved by modifying and tailoring the microstructure of sintered silicon nitride [23]. Additional work is currently underway to further understand the influence of process parameters on the evolving microstructure morphology like rod length, diameter, aspect ratio and ensuing properties using nanoscale Si_3N_4 and will be published separately. The calculated density of the sintered part was greater than 99% theoretical and the hardness was 1200 ± 50 HV1. The results from the test part confirm the quality of feedstock in obtaining sintered parts with good mechanical properties.

3. Design, simulation and optimization

Moldflow software developed by Autodesk Inc. was used for simulating the injection conditions. The selected part for simulation is from an engine design development by NWUAV Propulsion Systems. The top, side and isometric view of the part can be seen in Fig. 3. The measured feedstock properties were used an input for simulation studies. A three level three factorial Box–Behnken design of 15 different simulation runs with the individual process settings as shown in Table 2 was

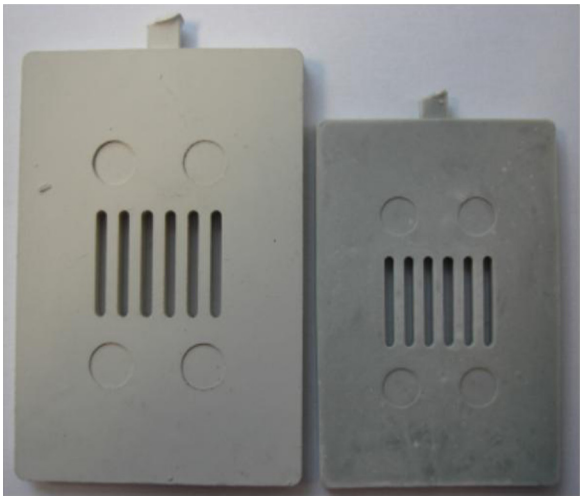

Fig. 1. Photograph of the injection molded (left) and sintered (right) validation part.

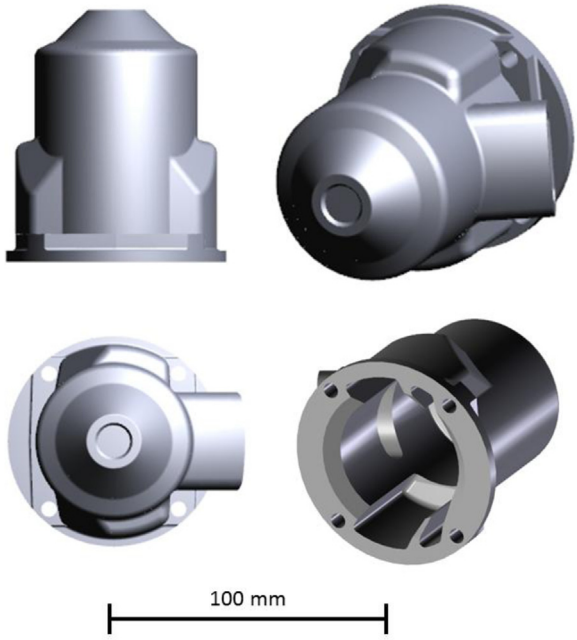

Fig. 3. The top, side and isomeric view of the engine part used in present simulation study.

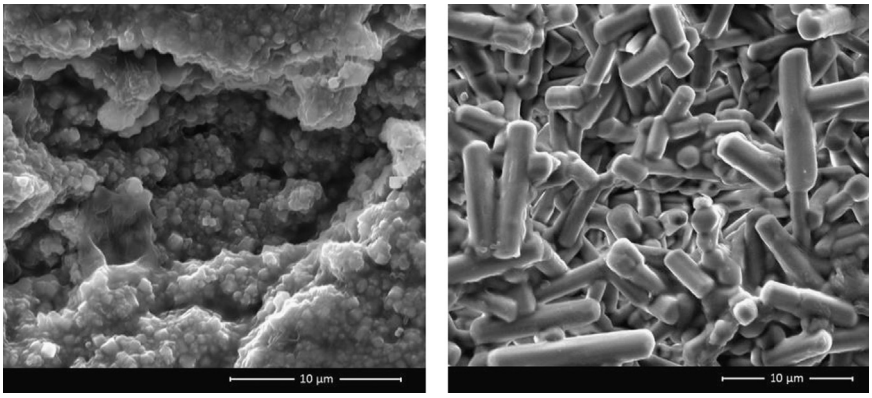

Fig. 2. SEM of the green (left) and sintered (right) microstructures of the validation part.

Table 2
Box–Behnken parameter settings used in the present study.

Run	Factors		
	Mold temperature (°C)	Melt temperature (°C)	Injection time (s)
1	150	23	0.16
2	150	33	0.16
3	150	23	0.24
4	150	33	0.24
5	180	23	0.16
6	180	33	0.16
7	180	23	0.24
8	180	33	0.24
9	150	28	0.20
10	180	28	0.20
11	165	28	0.16
12	165	28	0.24
13	165	23	0.20
14	165	33	0.20
15	165	28	0.20

analyzed to identify the critical process parameters. The design used in this work consists of 3 factors with 3 central points resulting in 10 coefficients for the quadratic model. The result from the Box–Behnken analysis performed for each quality criteria was expressed as a function of three process parameters (melt temperature, mold temperature and injection time).

The optimal injection molding parameters were further estimated using a non-linear programming (NLP) model. Lingo 13.0 (Lindo systems Inc., Chicago) was used to develop the NLP model. The optimization of the process parameters was based on the concept of reducing the differences between the absolute minimum and the current result of each quality criteria. This is achieved by minimizing the sum of all the differences where each difference is weighted the same. The quality criterion with a small percent of change over the range of the whole process window is weighted less. An NLP-model was built with an objective function, 27 variables and 20 non-linear constraints. These constraints contained all 10 surface responses.

Objective function:

$$\text{Min} \sum_{i-1}^{10} \Delta(Y_{Best}),\ Y(x_1, x_2, x_3)_i \tag{1}$$

Δ is the difference in percent between the result under optimal process parameters (x_1, x_2, x_3) for the quality criteria and the result with process parameters that are chosen with respect to other quality criteria as well.

Constraints:

$$Y_i = q_{i1} + q_{i2}c_1 + q_{i3}c_2 + q_{i4}c_3 + q_{i5}c_1^2 + q_{i6}c_1c_2 + q_{i7}c_1c_3 + q_{i8}c_2^2 + q_{i9}c_2c_3 + q_{i10}c_3^2$$

$$\Delta_i = (1 - Y_{Best}/Y_i) \times 100, \quad c_1 = \left(\frac{1}{15}x_1\right) - 11,$$

$$c_2 = (25x_2) - 5, \quad c_3 = \left(\frac{1}{5}x_3\right) - 5.6 \tag{2}$$

where, index i ranges from 1 to 10, quality criteria, x_1 is the melt temperature, x_2 is the injection time, x_3 is the mold temperature, q_{ij} is the quadratic RSM coefficient and c_k is the conversion coefficient.

4. Results and discussion

Feedstock properties such as viscosity, thermal conductivity, specific heat capacity, no-flow-temperature, the pressure–volume–temperature behavior and the solid and melt density were measured and used as input parameters to conduct PIM simulations. The results of the feedstock property measurements are summarized in Table 1. The detailed discussion regarding the observed trends in feedstock properties have been published elsewhere [3,22].

Initial simulations of the combustion engine part were carried out to understand the feasibility of injection molding the part successfully. A mold surface temperature of 28 °C, melt temperature of 165 °C and injection time of 0.2 s was chosen for the simulation of the engine part. The mesh created for simulation is shown in Fig. 4 and the parameters are summarized in Table 3. The fill behavior of the feedstock and the required time to fill the cavity is shown in Fig. 5.

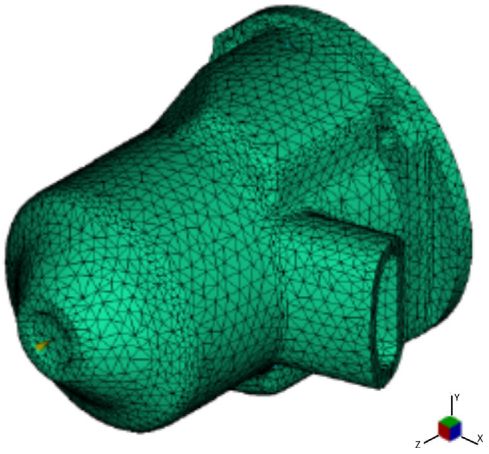

Fig. 4. Mesh geometry of the engine part.

Table 3
Mesh parameters used for simulation of engine part.

Attribute	Value
Mesh type	Fusion
Triangles	12732
Connected nodes	6358
Surface area	315 cm^2
Volume	62 cm^3
Maximum aspect ratio	21
Average aspect ratio	2
Minimum aspect ratio	1
Manifold edges	19098
Reciprocal percentage	80%
Match percentage	81%

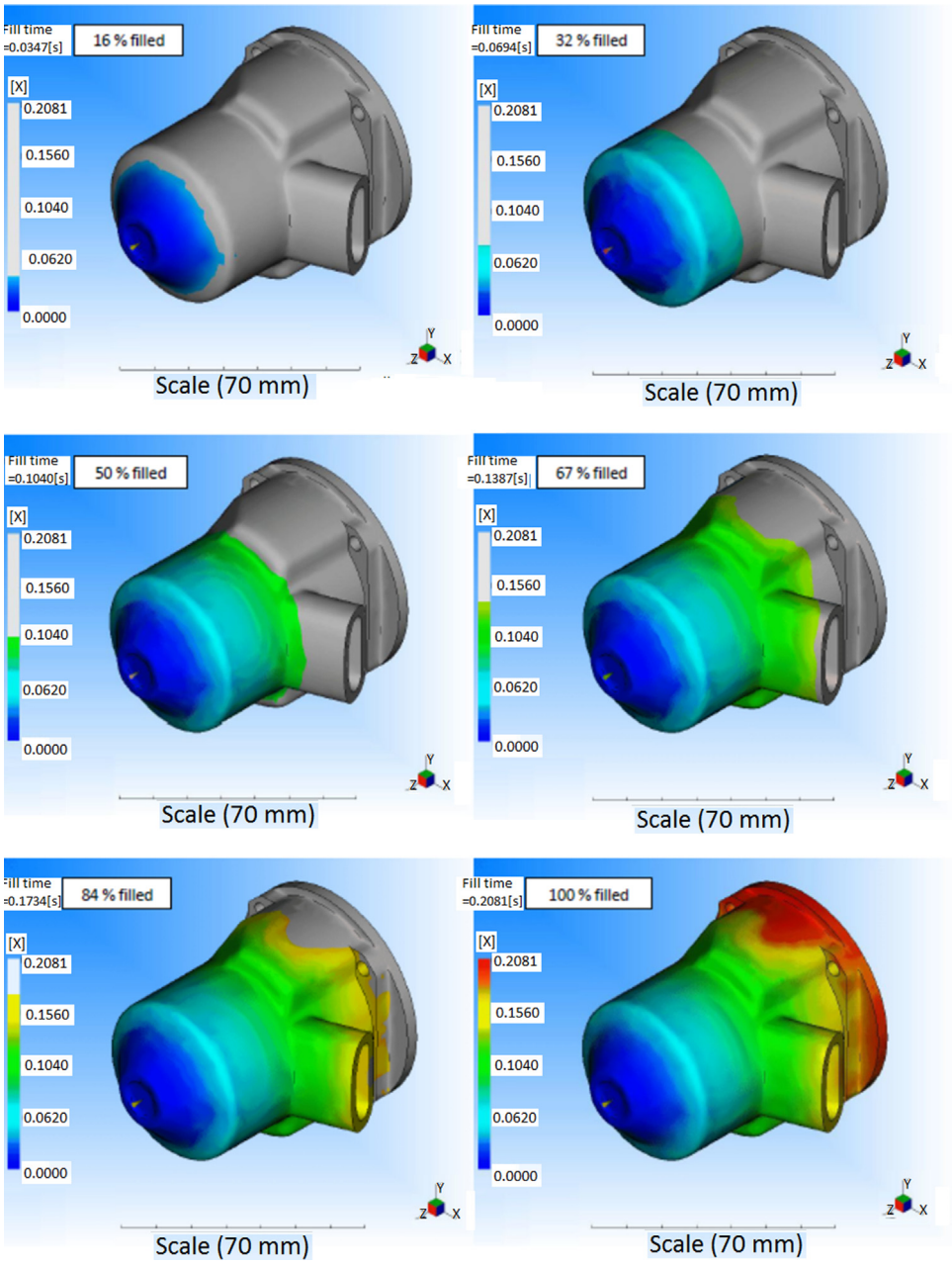

Fig. 5. Simulation of the fill behavior of the feedstock in the combustion engine mold cavity.

The simulations show smooth filling of the part without any observable defects.

The maximum pressure estimated in the simulation was 22 MPa at 0.2 s. The peak pressure was observed near the injection location. The maximum pressure for various commercially available injection molding machines typically range between 140 and 250 MPa [22]. The pressure needed was equivalent to one-eighth of the capabilities of a typical injection mold machine means multiple parts could be manufactured simultaneously. The clamp force is the product of area perpendicular to the mold dividing section and the pressure and is estimated to be 60 kN at 0.2 s. The clamp force of commercially available injection molding machines varies between 290 kN and 4500 kN [22]. The clamp force also shows fabrication of multiple parts simultaneously. The flow front temperature remained virtually unchanged (from 164.5 °C to 165 °C) from the injection of the material to the coldest point at the end of filling phase. The small difference between the highest and lowest temperature in the mold indicate the absence of hot or cold spots. As a guideline followed in the industry, a maximum drop of 2–5 °C in the flow front temperature is acceptable for preventing hot or cold spots. The areas susceptible for formation of weld lines and air traps are discussed elsewhere [3].

In order to obtain an initial process window, the lower bound of the mold temperature was explored with several simulation runs until a temperature was found where no short shots were formed. A short shot is the case when the feedstock melt

solidifies before the part is filled completely. Subsequently, the procedure was repeated for varying mold temperature. The upper bounds were chosen from the process recommendations provided by Datapoint Labs. This initial process window is shown in Fig. 6. This range was further used to analyze mold-filling behavior using optimization protocols.

In the present study, the Box–Behnken method was used to gain an understanding of critical parameters affecting the injection molding process. The simulation of variation of injection pressure (required pressure to squeeze the material into the cavity) for three different melt temperatures is shown in Fig. 7. A decrease in injection pressure with increase in melt temperature was observed. A low injection pressure is favored as it enables molding multiple parts in one stroke. Similar to injection pressure, the clamp force was also found to decrease with increase in melt temperature (Fig. 8). The clamp force is the force required to hold the two mold pieces together during the injection phase. The goal is to minimize the required force in order to produce as many parts as possible simultaneously. At the highest melt temperature (180 °C), the clamp force was found to decrease with increase in injection time. The simulation of bulk temperature for different injection times indicated a minimum bulk temperature at 180 °C melt temperature and at mold temperature between 23 and 29 °C.

The variation of shear stress for three different injection times is shown in Fig. 9. The shear stress during injection molding was found to be a minimum at an injection time of 0.16 s. A lower shear stress during injection molding is preferred to minimize the risk of powder binder separation. For 0.16 s injection time, the shear stress was found to be lowest at around 174 °C melt temperature and 26 °C mold temperature. Sink marks are an indicator for potential shrinkage due to a hot core. Sink marks were found to the lowest for high injection time and low mold temperature. It is desired to minimize sink mark depths. A high melt temperature and short injection time was found ideal for minimizing the temperature difference in the flow front. A low mold and melt temperature and high injection time resulted in lowest cooling time of the part.

Volumetric shrinkage is the percentage increase in local density from the end of the packing phase to the density at room temperature. The volumetric shrinkage was found to decrease with decrease in melt temperature. Analysis of the volumetric shrinkage for the lowest melt temperature of 150 °C showed that a short injection time and a high mold

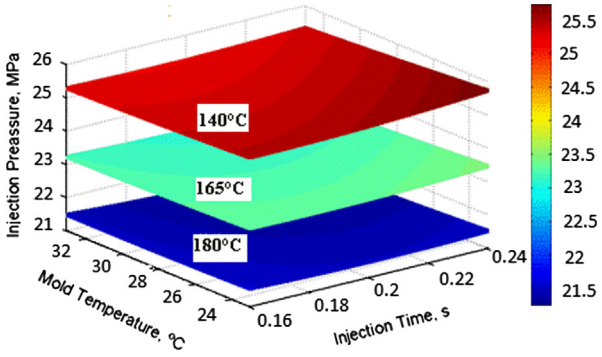

Fig. 7. Plot showing variation of injection pressure for three different planes of melt temperature plotted against the injection time and mold temperature.

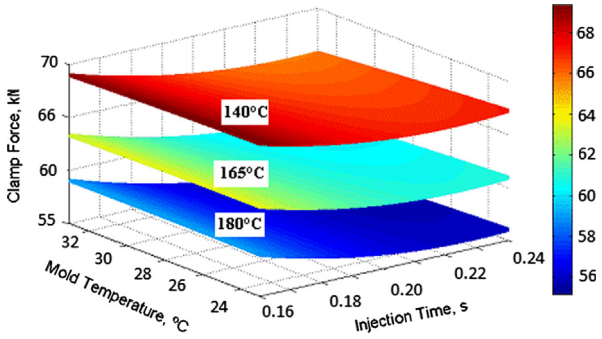

Fig. 8. Plot showing variation of clamp force for three different planes of melt temperature plotted against the injection time and mold temperature.

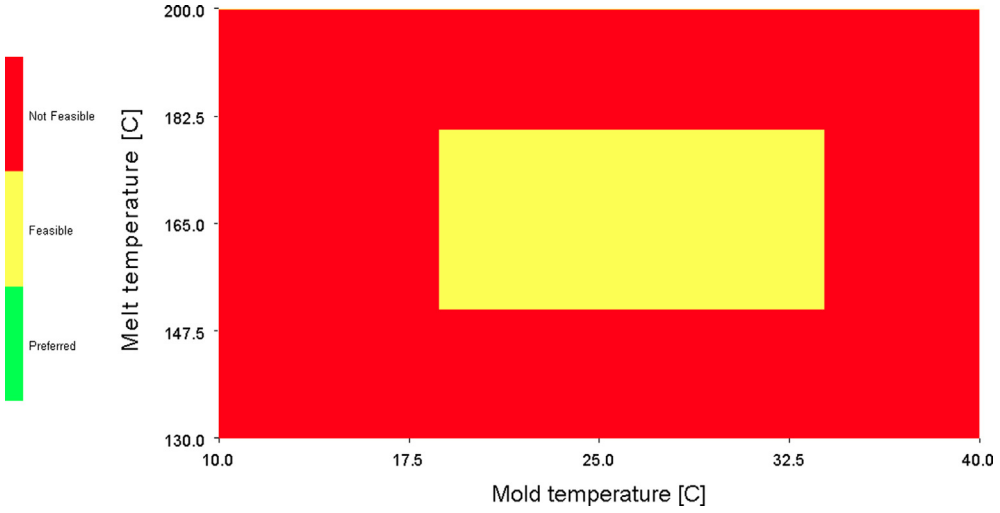

Fig. 6. An initial process window selected for simulation of the fill behavior of the feedstock in the combustion engine mold cavity.

temperature were preferable to minimize the volumetric shrinkage. The time at the end of packing is the sum of the fill time, the packing time and the holding time after pressure release for cooling. The time required should be minimized for efficient injection molding. The simulation results showed short time at the end of packing was for the lowest injection time. The simulation results also showed the lowest part weight was obtained at high melt and low mold temperature.

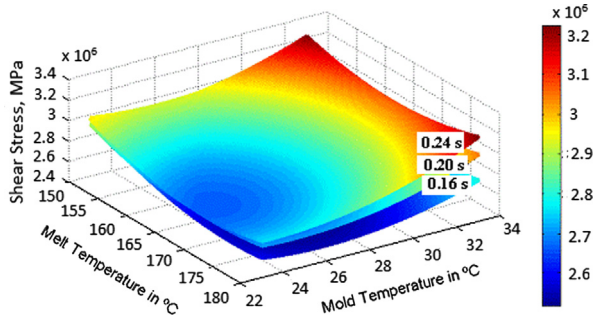

Fig. 9. Plot showing variation of shear stress for three different planes of injection time plotted against the melt and mold temperature.

Ten quality criteria were selected for further analysis. A summary of the minimal and maximal result and their difference percentage for each criterion is shown in Table 4. The process conditions to obtain the minimum for each criterion are shown in Table 5. The data in the table clearly shows that a single set of process parameters cannot be chosen to get the minimal for each quality criteria. The mold temperature was the dominant influence on the cooling time. The melt temperature was the dominant effect on the clamp force, injection pressure, shear stress, sink mark depth, temperature at flow front and volumetric shrinkage. The injection time was dominant factor for the bulk temperature and the time at the end of packing.

The NLP model identified an optimal combination of process parameters comprising of a melt temperature of 180 °C, an injection time of 0.16 s and a mold temperature of 23 °C. Fig. 10 shows the location of optimal processing conditions among various processing parameters. The results

Table 4
Range of each quality criterion obtained from mold-filling simulations.

Quality	Bulk temp. K (d)	Clamp force (N)	Pressure (MPa)	Stress (MPa)	Sink mark (mm)	Flow front K (d)	Cool time (s)	Shrink (%)	End of pack (s)	Wt. (Kg)
Min.	1.2	55100	21	2	0.3	0.06	11.1	1.1	30.1	0.1
Max.	1.4	69300	25	3	0.1	0.1	27.4	1.5	30.2	0.1
% Diff.	19.9	20	17	22	14.5	38	59.5	25.4	0.3	0.4

Table 5
Optimal process parameter settings for each criterion.

Quality	Bulk temp.	Clamp force	Pressure	Stress	Sink mark	Flow front	Cool time	Shrink	End of pack	Wt.
Melt temp. (°C)	180	180	180	173	150	180	150	150	168	180
Mold temp. (°C)	25	33	33	26	27	33	23	33	23	33
Injection time (s)	0.16	0.16	0.16	0.16	0.24	0.16	0.24	0.16	0.16	0.16

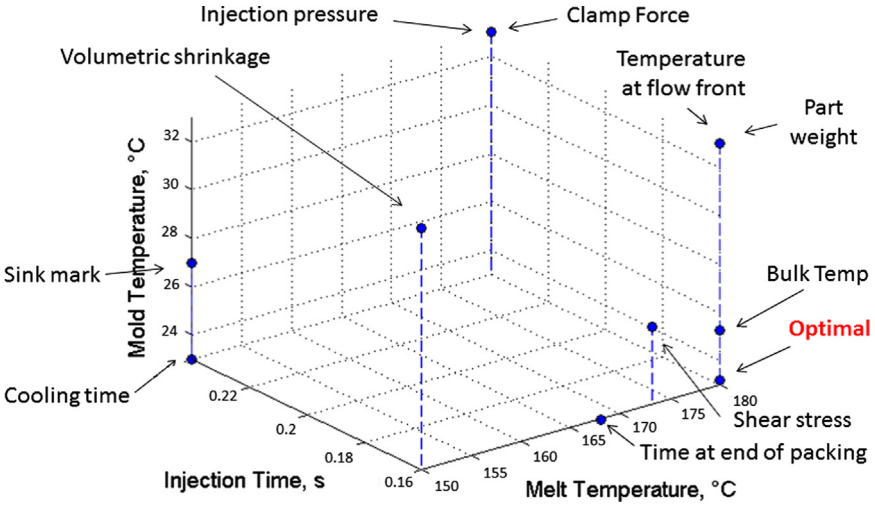

Fig. 10. Location of the optimal process conditions estimated from the NLP model.

Table 6
Results at optimized process parameters.

Quality	Bulk temp. K (d)	Clamp force (N)	Pressure (MPa)	Stress (MPa)	Sink mark (mm)	Flow front K (d)	Cool time (s)	Shrink (%)	End of pack (s)
Min.	1.2	55000	21.3	2.5	0.3	0.1	11.1	1.1	30.2
Opt.	1.4	59000	21.5	2.6	0.4	0.1	12.1	1.5	30.2
% Diff.	0.1	6.4	1.3	1.9	13.3	1.3	8.	24.2	0

of each quality criteria, the minimum and their range of variation are shown in Table 6.

5. Conclusions

A PIM feedstock consisting of nanosize Si_3N_4 powders mixed with magnesia, yttria and a paraffin wax–polypropylene binder system mixture was analyzed for its properties and molding attributes. The measured feedstock properties were used as input parameters for simulation of flow of material during injection molding process. The simulation results showed the melt temperature to be the dominant factor affecting the injection pressure, clamp force, shear stress, sink mark depth, temperature at flow front and volumetric shrinkage. Injection time was found to be the dominant factor effecting the bulk temperature and time at the end of the packing. Overall, the mold-filling simulations performed in the research study suggested the applicability of injection molding process to successfully fabricate engine components for UAV applications using nanoscale Si_3N_4. It is expected that the engineering community can use the simulation techniques discussed in the study to identify optimum processing conditions for fabricating the complex engine parts, thereby avoiding iterative expensive and time-consuming trials. The simulation techniques can also be used to evaluate the feasibility of manufacturing various critical parts by injection molding process.

References

[1] R.R. Sekar, R. Kamo, J.C. Wood, Advanced adiabatic diesel engine for passenger cars, SAE Paper, 1984, p. 840434.
[2] R. Kamo, W. Bryzik, Ceramics in heat engines, SAE Paper, 1979, p. 790645.
[3] J. Lenz, R.K. Enneti, V. Onbattuvelli, K. Kate, R. Martin, S. Atre, Powder injection molding of ceramic engine components for transportation, Journal of Metals 64 (2012) 388–392.
[4] M.H. Bocanegra-Bernal, B. Matovic, Mechanical properties of silicon nitride-based ceramics and its use in structural applications at high temperatures, Materials Science and Engineering A 527 (2010) 1314–1338.
[5] T. Takatori, T. Homma, N. Kamiya, H. Masaki, S. Sasaki, S. Wada, Fabrication and testing of ceramic turbine wheels, International Gas Turbine and Aeroengine Congress and Exposition, Orlando, Fl, USA, 3–6 June, 1991, ASME paper 91-GT-142.
[6] M.H. Bocanegra-Bernal, B. Matovic, Dense and near-net-shape fabrication of Si_3N_4 ceramics, Materials Science and Engineering A 500 (2009) 130–149.
[7] R.K. Enneti, T.S. Shivashankar, S.J. Park, R.M. German, S.V. Atre, Master debinding curves for solvent extraction of binders in powder injection molding, Powder Technology 228 (2012) 14–17.
[8] R.K. Enneti, S.J. Park, A. Schenck, R.M. German, P. Thomas, B. Levenfeld, A. Várez, I.O. Palagi de Souza, J.P. de Souza, A.M. Fuentefria, V. P. Onbattuvelli, S.V. Atre, Critical issues in manufacturing dental brackets by powder injection molding, International Journal of Powder Metallurgy 48 (2012) 23–28.
[9] K.H. Kate, V.P. Onbattuvelli, R.K. Enneti, S.W. Lee, S.J. Park, S. V. Atre, Measurements of powder–polymer mixture properties and their use in powder injection molding simulations for aluminum nitride, Journal of Metals 64 (9) (2012) 1048–1058.
[10] Y. Kobayashi, E. Matsuo, T. Inagaki, T. Ozawa Hot-gas spin testing of ceramic radial turbine rotor at TIT 1400 °C, SAE Paper, 1991, p. 910401.
[11] G.G. Vining, S.M. Kowalski, Statistical methods for engineers, Cengage Learning, Boston, USA, pp. 542–544.
[12] L. Wu, K.L. Yick, S.P. Ng, J. Yip, Application of the Box–Behnken design to the optimization of process parameters in foam cup molding, Expert Systems With Applications 39 (9) (2012) 8059–8065.
[13] M.A. Islam, M.R. Alam, M.O. Hannan, Multiresponse optimization based on statistical response surface methodology and desirability function for the production of particleboard, Composites Part B 43 (3) (2012) 861–868.
[14] A. Mirmohseni, S. Zavareh, Modeling and optimization of a new impact-toughened epoxy nanocomposite using response surface methodology, Journal of Polymer Research 4 (18) (2012) 509–517.
[15] L. Huiping, Z. Guoqun, N. Shanting, L. Yiguo, Technologic parameter optimization of gas quenching process using response surface method, Computational Materials Science 38 (4) (2007) 561–570.
[16] K. Velmanirajan, A.T.A. Syed, R. Narayanasamy, B.C. Ahamed, Numerical modelling of aluminium sheets formability using response surface methodology, Materials Design 41 (2012) 239–254.
[17] L.M. Galantucci, R. Spina, Evaluation of filling conditions of injection molding by integrating numerical simulations and experimental tests, Journal of Materials Science and Technology 141 (2) (2003) 266–275.
[18] K. Wang, J. Li, R.G. McDonald, R.E. Browner, The effect of iron precipitation upon nickel losses from synthetic atmospheric nickel laterite leach solutions: statistical analysis and modeling, Hydrometallurgy 109 (1–2) (2011) 140–152.
[19] S.K. Tripathy, Y. Rama Murthy, Modeling and optimization of spiral concentrator for separation of ultrafine chromite, Powder Technology 221 (2012) 387–394.
[20] A. Mäntynen, A. Zakharov, S.L. Jämsä-Jounela, M. Graeffe, Optimization of grinding parameters in the production of colorant paste, Powder Technology 217 (2012) 216–222.
[21] R.B. Heimann, Better quality control: stochastic approaches to optimize properties and performance of plasma-sprayed coatings, Journal of Thermal Spray Technology 19 (4) (2010) 765–778.
[22] J. Lenz, Materials and Process Design for Powder Injection Molding of Silicon Nitride for the Fabrication of Engine Components, Oregon State University, Corvallis, Oregon, USA, 2012 (MS thesis).
[23] L.A. Geneova, V.A. Izhevskyi, C.J. Bressiani, Effect of processing variables on synthesis of β-Si_3N_4 particles, Journal of the European Ceramic Society 28 (2008) 295–301.
[24] P. Sajgalik, J. Dusza, M.J. Hoffmann, Relationship between microstructure, toughening mechanisms, and fracture toughness of reinforced silicon nitride ceramics, Journal of the American Ceramic Society 78 (1995) 2619–2624.
[25] B. Wang, J. Yang, R. Guo, J.Q. Gao, J.F. Yang, Microstructure characterization of hot-pressed β-silicon nitride containing β-Si_3N_4 seeds, Materials Characterization 60 (2009) 894–899.
[26] D.A. Gould, M. Quinlan, M.P. Albano, L.B. Garrido, L.A. Genova, K. P. Plucknet, A simple method for synthesis of acicular b-Si_3N_4 seed crystals, Ceramics International 35 (2009) 1357–1362.